



Ba-vacancy induces semiconductor-like photocatalysis on insulator BaSO₄

Wen Cui^a, Lvcun Chen^a, Jieyuan Li^{b,d}, Ying Zhou^a, Yanjuan Sun^{b,c}, Guangming Jiang^{b,c}, S.C. Lee^e, Fan Dong^{a,b,*}



^a The Center of New Energy Materials and Technology, School of Materials Science and Engineering, Southwest Petroleum University, Chengdu 610500, China

^b Research Center for Environmental Science & Technology, Institute of Fundamental and Frontier Sciences, University of Electronic Science and Technology of China, Chengdu 611731, China

^c Chongqing Key Laboratory of Catalysis and New Environmental Materials, College of Environment and Resources, Chongqing Technology and Business University, Chongqing 400067, China

^d College of Architecture and Environment, Sichuan University, Chengdu, Sichuan, 610065, China

^e Department of Civil and Environmental Engineering, The Hong Kong Polytechnic University, Hong Kong, China

ARTICLE INFO

Keywords:

Ba-vacancy
Insulator
Semiconductor-like photocatalysis
Catalytic mechanism
Solar energy conversion

ABSTRACT

Semiconductor-based photocatalysis has attracted considerable interdisciplinary attention for its diverse applications in environmental remediation and solar energy conversion. However, pure earth-abundant insulators have been seldom considered as photocatalysts because of the unfeasible electronic excitation. In this work, we make the earth-abundant insulator BaSO₄ as conceptually new photocatalyst via Ba-vacancy engineering for the first time. The BaSO₄ with Ba-vacancy is synthesized by a facile precipitation method and applied for photocatalytic NO removal in air. XAFS spectroscopy and DFT calculations demonstrate the formation of Ba-vacancy. Also, defect level induced by Ba-vacancy between the wide band gap is demonstrated, which endows insulator BaSO₄ with semiconductor-like photocatalytic performance. Besides, according to the TPD analysis and theoretical simulation, Ba species is functioned as the NO_x storage center for the primary accumulation of NO molecule on substrate, and simultaneously Ba-vacancy is equipped with the capability to redistribute charge carriers and thus accelerate the activation of NO molecule by the donation of electrons to electron-deficient areas, facilitating the conversion of NO into a higher valance state for further favorable photocatalytic oxidation. In situ DRIFTS spectra are applied to dynamically monitor intermediates and products on photocatalyst surface, revealing the reaction process and the enhancement role of Ba-vacancy. This work opens a new research doorway on earth-abundant insulators for the development of a new family of photocatalyst.

1. Introduction

This is the age where the capture and utilization of solar energy for energy conversion has attracted considerable interdisciplinary attention [1–3]. Heterogeneous photocatalysis, which could use the photo-induced charge carriers inside a material as a working medium to realize the conversion of solar energy, has been investigated and developed extensively in response to addressing the energy and environmental issues [4–8]. There are numerous research works dealing with the topic of the design of highly efficient semiconductor-based photocatalysts [9–14]. Meanwhile, some insulator-related materials also have been exploited, including photocatalytic NO removal on insulator-based heterojunctions, selective photo-oxidation of different benzyl alcohols in the presence of a large variety of dyes and O₂ on aluminum oxide,

and photo-induced H₂ production on insulator quartz surfaces [15–18]. However, the pure earth-abundant insulators with metal-defects have never been reported probably because of the unfeasible electronic excitation on insulator [19].

During heterogeneous photocatalysis, the adsorption of reactive molecules, the photoactivated reaction, and the desorption of product molecules are the elementary processes mediated by the substrate and correspondingly determine the feasibility and efficiency of photocatalytic reaction [20–23]. Considering this fact, appropriate modification could endow insulator with semiconductor-like photocatalysis, realizing the direct conversion of solar energy to chemical energy on earth-abundant materials [15–19]. Recent years have witnessed fruitful studies on electronic structure tailoring and catalytic performance enhancement. The vacancy-engineering is one of the most studied and

* Corresponding author at: The Center of New Energy Materials and Technology, School of Materials Science and Engineering, Southwest Petroleum University, Chengdu 610500, China.

E-mail address: dfctbu@126.com (F. Dong).

effective methods that could manipulate the properties of materials such as surface structure, electrical transport and band structures. This could introduce the insulators with new features and functions [24–26].

In this work, vacancy-engineering is proposed to make the pure earth-abundant insulator as photocatalyst and the BaSO₄ with Ba-vacancy (BSO) is synthesized by a facile precipitation method and applied for photocatalytic NO removal. For the first time, we discover that defect level induced by Ba-vacancy between the wide band gap endows insular BaSO₄ with semiconductor-like photocatalysis. Meanwhile, Ba species is functioned as the NO_x storage centre for the primary accumulation of NO molecule on substrate, and simultaneously Ba-vacancy is equipped with the capability to redistribute charge carriers and thus accelerate the activation of NO molecule by the donation of electrons to electron-deficient areas, facilitating the conversion of NO into a higher valance state for further favorable photocatalytic oxidation. Reaction process and the enhancement role of Ba-vacancy also have been revealed by *in situ* diffuse reflectance infrared Fourier transform spectroscopy (DRIFTS). This work opens a new research doorway on earth-abundant insulator for the development of a new family of photocatalyst.

2. Experimental

2.1. Synthesis of defect-controlled BaSO₄

All the reagents employed in this study were analytical grade and used without further purification. BaSO₄ was obtained by a simple precipitation method. 10 mmol Ba(NO₃)₂ dissolved in 60 mL deionized water was added dropwise into 70 mL aqueous solutions of Na₂SO₄, which were mixed together in 1:1 M ratio and stirred for 1 h. For exploring the influence on reaction temperature, three different samples have been synthesized at room temperature (20 °C), 40 and 80 °C in a water bath. Afterward, the precipitates were washed by deionized water and ethanol four times and dried at 60 °C. The samples which were synthesized at room temperature, 40 and 80 °C are labelled as BSO, BSO-40 and BSO-80, respectively. Commercial BaSO₄ (PBSO) with rare defects purchased from Aladdin Industry Corporation.

2.2. Evaluation of photocatalytic activity

The photocatalytic activity was investigated by examining the removal ratio of NO at ppb levels (500 ppb) in a continuous-flow reactor (rectangular reactor, 30 cm × 15 cm × 10 cm). The concentration of NO was continuously detected by a NO_x analyzer (Thermo Environmental Instruments Inc., model 42c-TL). 0.20 gas-prepared sample was dispersed and coated onto two glass dishes (diameter: 12.0) for photocatalytic activity tests under UV-light irradiation ($\lambda = 280$ nm). After adsorption-desorption equilibrium being achieved, the lamp was turned on and the removal ratio (η) of NO was calculated as $\eta = (1 - C/C_0) \times 100\%$, where C and C_0 are the concentrations of NO pollutant in the outlet steam and the feeding stream, respectively.

After the photocatalytic NO oxidation test, the post-tested sample was washed by 35 mL deionized water and then the supernatant was collected to analyze the content of accumulated final products. Gas-phase molecular absorption spectrometer (GMA3370), which is a specific analytical technique applied to measure nitrite nitrogen, nitrate nitrogen, total nitrogen and so on, was used to quantitatively detect the content of NO₂⁻/NO₃⁻ species on post-test samples.

2.3. In situ DRIFTS investigation

In situ DRIFTS measurements were conducted using a TENSOR II FT-IR spectrometer (Bruker) equipped with an *in situ* diffuse-reflectance cell (Harrick) and a high-temperature reaction chamber (HVC), as shown in Scheme S1. Detailed descriptions of the *in situ*

DRIFTS apparatus are available in the Supplementary Material.

Before measurements, the prepared samples were pretreated 30 min at 300 °C in the high-temperature reaction chamber. The background spectra were recorded before injecting reactant gas into the reaction chamber. The total gas flow rate was 100 mL/min, and the concentration of NO was adjusted to 50 ppm by dilution with O₂. Once the adsorption equilibrium was achieved, a UV-light source was applied to initiate the photocatalytic reaction. The temporal evolution of normalized absorbance of adsorbed NO₂⁻/NO₃⁻ species on photocatalysts surface correspond with *in situ* DRIFTS spectra, and the integration of characteristic absorption bands of adsorbed species leads to follow their individual evolutions as a function of time. For all species, the normalized absorbance is calculated by considering their individual maximum absorbance as 1.

3. Results and discussion

3.1. Chemical composition and microstructure

The X-ray diffraction (XRD) patterns indicate that as-synthesized BaSO₄ with Ba-vacancy (BSO) well maintains the orthorhombic structure of BaSO₄ (PDF#24-1035). However, a decreased degree of crystallinity can be observed in comparison with commercial BaSO₄ (PBSO, purchase from Aladdin Industry Corporation), attributing to the low crystallization with the potential formation of defect. We subsequently employ a powerful element-specific tool, the synchrotron radiation-based X-ray absorption fine structure (XAFS) spectroscopy, to characterize the defect-controlled BaSO₄, using PBSO sample with rare defects as a reference. Although there is a general similarity of Ba L3-edge X-ray Absorption Near Edge Structure (XANES) for BSO and PBSO samples, [27] an obvious shift of adsorption edge towards to higher photon energy can be observed. This result indicates a decreased electron concentration in BSO crystal and thus demonstrating the formation of the Ba-vacancy inducing coordinatively unsaturated sites [28]. Meanwhile, the high-resolution spectrum of Ba 3d with peak features at 795.9 eV (Ba 3d_{3/2}) and 780.2 eV (Ba 3d_{5/2}) presents a right shift of adsorption peaks toward lower binding energy in BSO sample, indicating the existence of Ba-vacancy on BaSO₄, which is also corresponding to the XANES spectra. [29] Ignited by this observation, detailed atomic-level structures of defect-controlled samples are simulated by Density Functional Theory (DFT) calculations. As shown in Fig. 1d-f, the optimized geometric structure of BaSO₄ with Ba-vacancies, O-vacancy and SO₄-vacancy are simulated respectively for comparison. The lowest formation energy (E_f) of the BaSO₄ with Ba-vacancy demonstrates that the formation of Ba-vacancy in BaSO₄ lattice is most attainable. Thus, the highly combined and complementary experimental characterization and theoretical simulation confirm the construction of Ba-vacancy in BaSO₄ lattice.

The morphological feature of the as-prepared defect-controlled samples was further studied by scanning electron microscopy (SEM) and high-resolution transmission electron microscopy (HRTEM). The as-prepared samples exhibit nanoparticle morphology (Fig. 2a,b) and EDX elemental mapping of BSO sample suggests that the S, O, and Ba elements are distributed uniformly. Nevertheless, a slight lattice disorder and dislocation can be locally observed in the margin of BSO sample (circled by dotted line in Fig. 2d), highlighting the existence of vacancy. [30] According to the XPS analysis, the atomic ratio of sulfur to barium (S/Ba) and oxygen to barium (O/Ba) in PBSO sample are both smaller than that of in BSO sample, which also indicates the formation of Ba-vacancy in BSO. Additionally, the nature of Ba-vacancy was further resolved by room temperature solid state electron paramagnetic resonance (EPR) spectroscopy. The defect-rich BSO sample displays a much higher EPR signal intensity (g value is 2.0028, Fig. 2e) both in dark and under UV-light irradiation, which can be identified as the electrons trapped around Ba-vacancy. A weak EPR signal has been detected in PBSO sample due to the inevitably intrinsic defects in

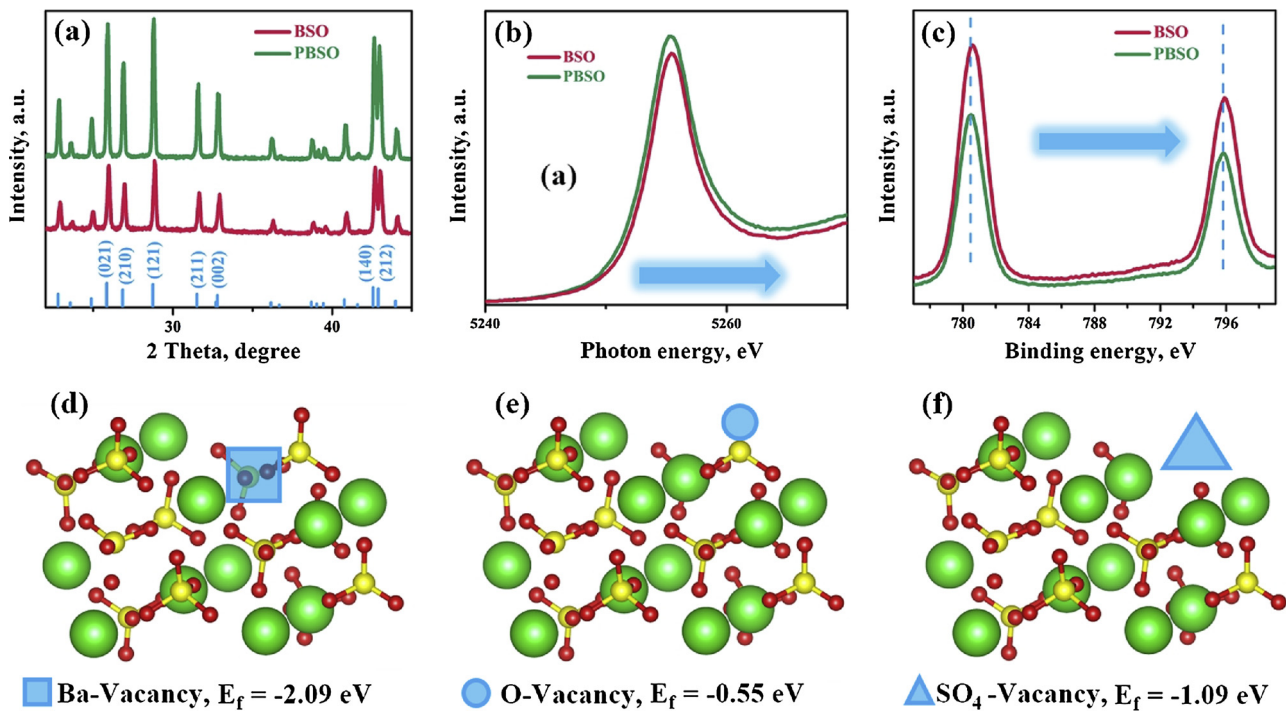


Fig. 1. Structural characterization for the defect-controlled samples. XRD pattern (a), the normalized X-ray absorption near-edge structure (XANES) spectra (b), and high-resolution (Ba 3d) XPS spectra (c) of BSO and PBSO samples; and schematic illustrating the locations of Ba-vacancy (d), O-vacancy (e), SO₄-vacancy (f) in BaSO₄ lattice. E_f stands for the formation energy of the optimized geometric structure, negative values indicate heat release. Green, red and yellow spheres stand for Ba, O and S atoms, respectively. (For interpretation of the references to colour in this figure legend, the reader is referred to the web version of this article).

material, [26] which is also the reason why commercial PBSO exhibits a low photocatalytic activity.

3.2. Optical properties and band structures

The photo-absorption property of defect-controlled samples were studied by UV-vis diffuse-reflectance spectrometry (UV-vis DRS) spectra, using a scanning UV-vis spectrophotometer equipped with an integrating sphere assembly and 100% commercial BaSO₄ as the reflectance sample. Surprisingly, defect-rich BSO sample demonstrates strong light absorption with the absorption edge located at approximately 254 nm. The corresponding experimental value of the bandgap (4.89 eV) is well consistent with the reported value, and also indicates that BaSO₄ is a typical insulator with wide band gap. Besides, it's worth noting that a weak absorption peak centered around 270–300 nm can be clearly observed. Combining with the experimental characterization and theoretical simulation, it can be concluded that this special optical absorption characteristics originate from the defect state emission that derives from the Ba-vacancy. The position of defect level is thus estimated via a plot of $(\alpha h\nu)^{1/2}$ versus photon energy ($h\nu$), as shown in Fig. 3a (inset). Furthermore, the total density of states (TDOS) are calculated by DFT method (Fig. 3b), which shows a tolerable error in comparison with the experimental value. [31] A middle energy level (at 3.8 eV) below the conduction band (CB) appears in the band gap structure of BSO (marked by shaded area). According to the calculation of partial density of states (PDOS), the contribution of the 3d states of Ba atoms on account of the presence of Ba-vacancy. In this case, photoexcited electrons could easily jump from a foothold (valence band) to the springboard (middle defect level) under irradiation. This electronic transition induces insular BaSO₄ with photocatalytic performance, similar to the semiconductor photocatalysis. Therefore, the Ba-vacancy plays a vital role in band structure engineering and facilitating the electronic excitation under irradiation. The deductive band structure of defect-controlled BSO sample is shown in Fig. 3c.

3.3. Adsorption and activation of NO molecule and photocatalytic performance

Furthermore, the Ba-vacancy, as the essence for the semiconductor-like photocatalytic performance on insulator BaSO₄, could provide unsaturated sites to facilitate the adsorption and activation of reactant. The adsorption of reactants on the surface of catalyst, as the precondition of heterogeneous catalysis, should be well promoted in order to ensure the subsequent catalytic reaction. Exactly, the Ba species are equipped with the performance of NO_x storage, which has been well demonstrated by the temperature-programmed desorption (TPD) profiles (Fig. 4a). [32,33] Obviously, BSO sample shows a much stronger adsorption capability than that PBSO, which indicates that Ba-vacancy could accelerate the adsorption of NO molecule on the defective site. Meanwhile, as depicted by the charge difference density (Fig. 4a, inset), the Ba-vacancy makes the local charge redistributed by serving as convergent center of electrons to assemble delocalized electrons to form localized states, which is beneficial to facilitate the adsorption and activation of reactant on/around defect site. The adsorption and activation of NO molecule are subsequently probed by DFT calculations. As shown in Fig. 4b, the NO molecules tend to absorb on the side of defect site. The increased adsorption energy (from -1.03 eV for PBSO to -1.67 eV for defect-controlled BSO) implies that the adsorption of NO is promoted on BSO. The total charge of NO for BSO sample ($\Delta q = 0.41$ e, calculated with Bader method [34]) indicates that the NO molecules would donate electrons to electron-deficient areas (around the defect sites) to form NO⁺ species, promoting the activation of NO molecule and thus inducing the conversion NO into a higher valance state for further favorable photocatalytic oxidation. Therefore, the construction of Ba-vacancy could not only induce the semiconductor-like photocatalytic performance on insulator BaSO₄ but also facilitate the adsorption and activation of gas molecule for NO removal.

Consequently, to experimentally characterize the adsorption and activation of reactant, in situ DRIFTS was used to dynamically monitor intermediates and products on photocatalyst surface during NO

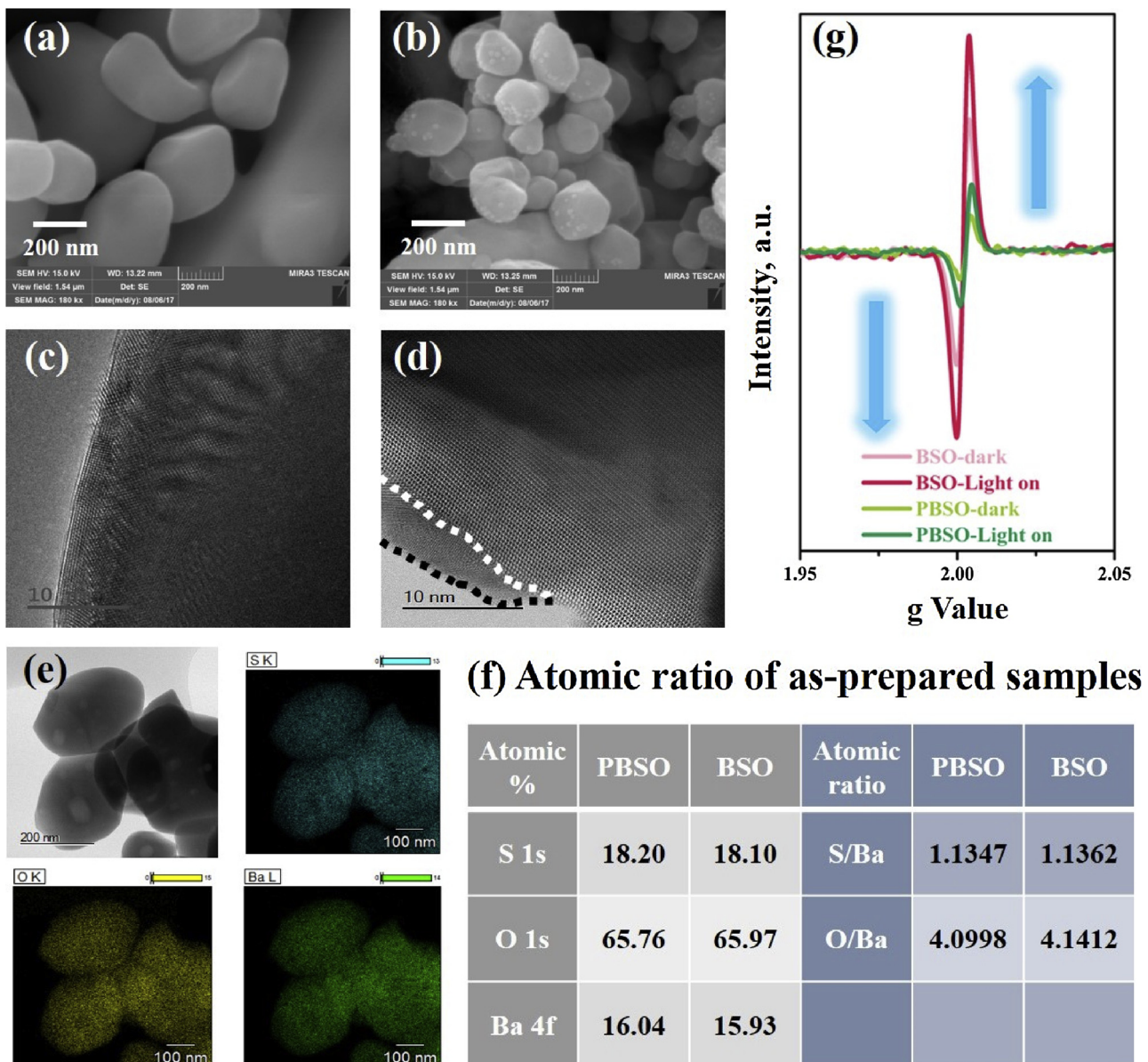


Fig. 2. Microstructure of the catalysts. SEM and HRTEM images of PBSO (a, c) and BSO (b, d); EDX elemental mapping of S, O, and Ba in image for BSO sample (e); atomic ratio of BSO and PBSO samples (f); and room temperature solid state EPR spectra (g) of as-prepared samples.

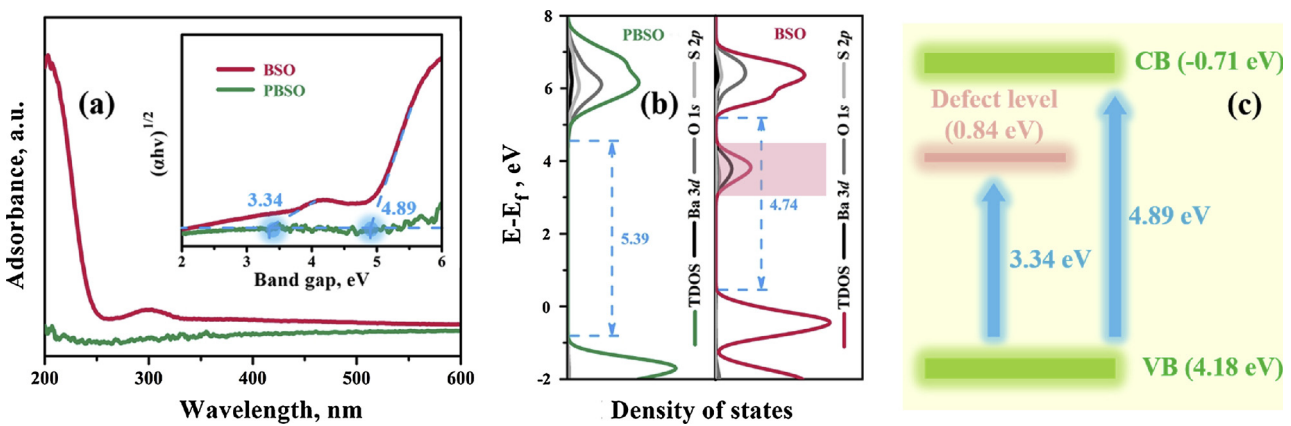


Fig. 3. The photo-absorption property and band structure. The UV-vis spectra and the estimated plot of $(\alpha h\nu)^{1/2}$ versus photon energy (inset) of prepared samples (a); density of states (DOS), the Fermi level is set to 0 eV (b); and the deductive band structure of defect-controlled BSO sample (c).

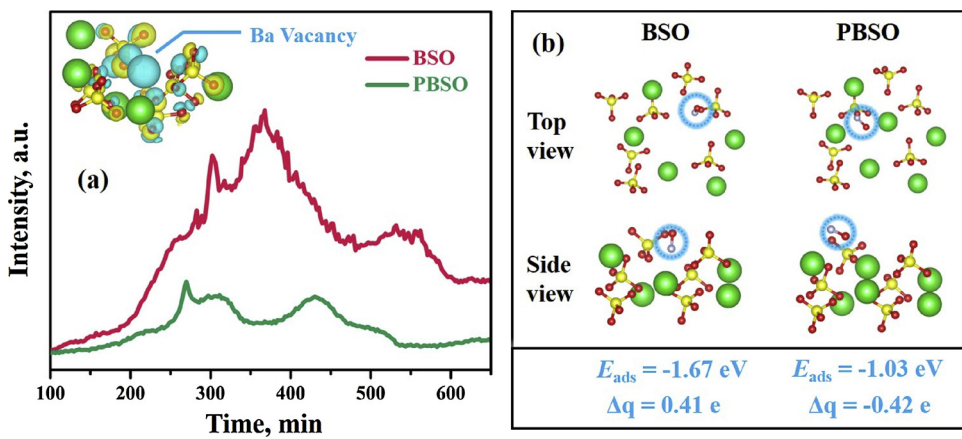


Fig. 4. Adsorption and activation of NO molecules. TPD profiles of BSO and PBSO for NO gas (a), and charge difference density distribution of BSO (Fig. 4a, insert): charge accumulation is shown in blue and depletion in yellow, and isosurfaces are set to 0.002 eV Å⁻³; optimized geometric structure of NO molecules adsorption on BSO and PBSO (b). Green, red, yellow and gray spheres stand for Ba, O, S and N atoms, respectively. (For interpretation of the references to colour in this figure legend, the reader is referred to the web version of this article).

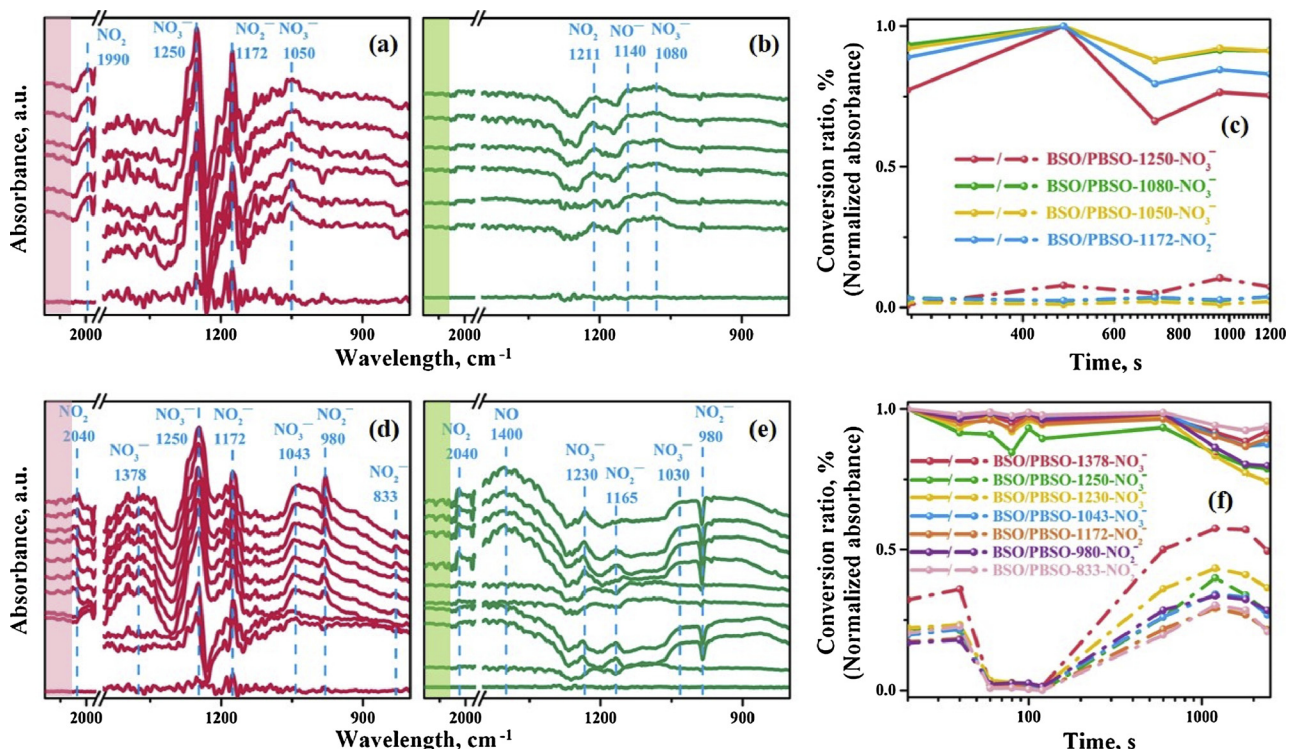


Fig. 5. In situ DRIFTS spectra of BSO and PBSO samples. In situ DRIFTS spectra on BSO and PBSO samples during NO adsorption (a, b) and UV-light irradiation (d, e) processes, respectively; temporal evolution of normalized absorbance of adsorbed NO₂⁻/NO₃⁻ species on BSO (solid line,) and PBSO (dashed line,) during NO adsorption (c) and UV-light irradiation (f) processes, corresponding to in situ DRIFTS spectra.

adsorption and UV-light irradiation processes. As shown in Fig. 5a and b, the absorption bands related to NO species on BSO obviously appear once NO was introduced at 25 °C in dark conditions in comparison with PBSO. Note that the absorption band approximately around 2120 cm⁻¹ (marked by shaded area) associated with nitrosyl species (NO⁺) over BSO sample arises gradually as evidenced by the DFT calculation. [35] This is consistent with the theoretical results that the construction of Ba-vacancy could accelerate the activation of NO molecule by the donation of electrons of NO molecule to electron-deficient areas, and thus facilitating the conversion of NO into NO⁺ during the adsorption stage. Also, the dark reactions about the generation of NO₂⁻/NO₃⁻ (the absorption band around at 1900, 1250, 1172, 1050 cm⁻¹) [36–38] have been extremely promoted due to the localized center of electrons around Ba-vacancy, as suggested by the evolution of the normalized absorbance of NO₂⁻/NO₃⁻ species (Fig. 5c). Besides, the time-dependent IR spectra of BSO and PBSO under UV-light irradiation are recorded once the adsorption equilibrium is achieved (Fig. 5d and e). And

the “baseline” spectrum is the same as that of “the curve of adsorption equilibrium” in NO adsorption process. The distinct absorption bands about NO₂⁻/NO₃⁻ (at 1378, 1250, 1172, 1043, 980, 833 cm⁻¹) [36,37,39,40] can be observed on BSO, reflecting that the amount of final products (nitrites or nitrates) generated on BSO is much higher than that on PBSO, which is accordance with the temporal evolution of normalized absorbance of NO₂⁻/NO₃⁻ on samples (Fig. 5f). Therefore, Ba-vacancy as the activate sites could significantly promote the adsorption and activation of reactants, and thus enhance the photocatalytic NO removal efficiency.

The photocatalytic performance of prepared samples towards NO removal was evaluated under UV-light irradiation ($\lambda = 280$ nm). As shown in Fig. 6a, the commercial PBSO exhibits a slight photocatalytic NO removal performance, arising from the inevitably intrinsic defects and the capability of NOx storage on Ba species. The photocatalytic NO removal efficiency of defect-controlled BSO sample is increased to 42.0%. Besides, according to the Fig. S4, higher reaction temperature

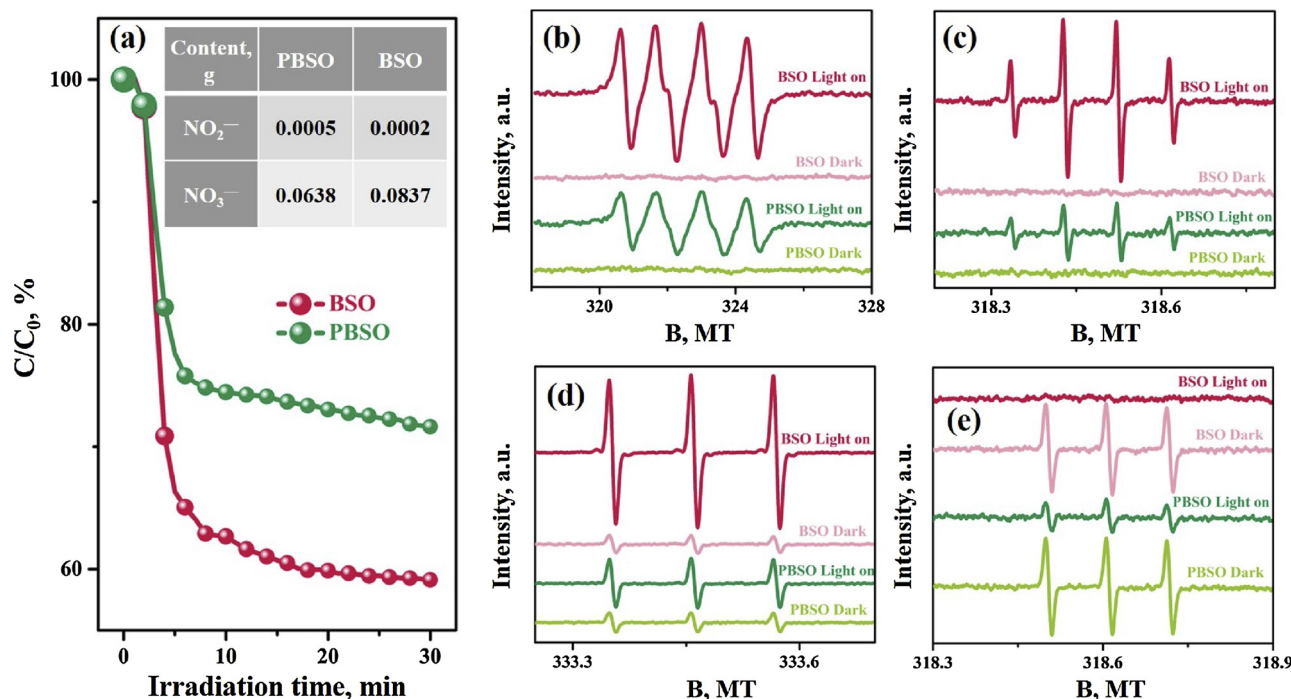


Fig. 6. Evaluation and analysis of the photocatalytic performance. Photocatalytic activity comparison (a), the content of NO_2^- and NO_3^- species on post-test BSO and PBSO samples (Fig. 6a, insert); and DMPO spin-trapping ESR spectra of BSO and PBSO samples, $\cdot\text{O}_2^-$ (b), $\cdot\text{OH}$ (c), $^1\text{O}_2$ (d), e^- (e).

could accelerate the crystallization of samples and thus reduce the formation of defects, giving rise to decreased photocatalytic efficiencies in comparison with BSO sample. Also, the final products ($\text{NO}_2^-/\text{NO}_3^-$) has been verified and quantitatively detected by gas-phase molecular absorption spectrometer. As shown in Fig. 6a (insert), NO_3^- species is the major final product both in BSO and PBSO samples and the content of NO_3^- species on BSO is much higher than that of on PBSO. The photocatalytic NO oxidation is achieved by the photo-induced reactive radicals. As noted, in comparison with PBSO, much stronger DMPO spin-trapping signals of reactive oxygen species (ROS, superoxide anion radical ($\cdot\text{O}_2^-$, Fig. 6b), hydroxyl radical ($\cdot\text{OH}$, Fig. 6c), and singlet oxygen ($^1\text{O}_2$, Fig. 6d)) have been detected for BSO. Correspondingly, the signals of trapped electrons (e^- , Fig. 6e) on BSO are reduced as the consumed electrons are transformed into the ROS. [41] Therefore, Ba-vacancy induces the formation of defect level to endow the insular BaSO_4 with semiconductor-like performance, and simultaneously serves as the active center to significantly promote the reactants activation for optimized photocatalysis.

4. Conclusions

In conclusion, we develop the BaSO_4 with intrinsic Ba-vacancy for the first time and investigate the essence for the insulator with semiconductor-like performance. The construction of Ba-vacancy contributes to the formation of defect level to enable photocatalytic performance on insulator BaSO_4 and simultaneously manipulates the band structure, surface property, and charge carrier redistribution of BSO. The multiple roles of Ba-vacancy give rise to unprecedented photocatalytic performance on BaSO_4 in removal of NO in air. This work proposes a new concept on photocatalysis with earth-abundant insulators. The discovery of this interesting semiconductor-like photocatalysis induced by defects would motivate further work in this field, which could carve a potential path for the practical viability in the development of environmental and energy-related applications.

Acknowledgements

This work was supported by the National Natural Science Foundation of China (21822601, 21777011 and 21501016), the National Key R&D Plan (2016YFC02047), the Innovative Research Team of Chongqing (CXTDG201602014), the Key Natural Science Foundation of Chongqing (cstc2017jcyjBX0052) and the Plan for "National Youth Talents" of the Organization Department of the Central Committee. The authors also acknowledge the AM-HPC in Suzhou, China for computational support.

Appendix A. Supplementary data

Supplementary material related to this article can be found, in the online version, at doi:<https://doi.org/10.1016/j.apcatb.2019.04.070>.

References

- [1] C. George, M. Ammann, B. D'Anna, D.J. Donaldson, S.A. Nizkorodov, Heterogeneous photochemistry in the atmosphere, *Chem. Rev.* 115 (2015) 4218.
- [2] X. Zhang, M. Fevre, G.O. Jones, R.M. Waymouth, Catalysis as an enabling science for sustainable polymers, *Chem. Rev.* 118 (2017) 839–885.
- [3] J. Baxter, Z. Bian, G. Chen, D. Danielson, M.S. Dresselhaus, A.G. Fedorov, T.S. Fisher, C.W. Jones, E. Maginn, U. Kortshagen, Nanoscale design to enable the revolution in renewable energy, *Energy Environ. Sci.* 2 (2009) 559–588.
- [4] M.R. Hoffmann, W. Choi, D.W. Bahnemann, Environmental Applications of semiconductor photocatalysis, *Chem. Rev.* 95 (1995) 69–96.
- [5] H. Tong, S. Ouyang, Y. Bi, N. Umezawa, M. Oshikiri, J. Ye, Nano-photocatalytic materials: possibilities and challenges, *Adv. Mater.* 24 (2012) 229.
- [6] K. Dohyung, K.K. Sakimoto, H. Dachao, Y. Peidong, Artificial photosynthesis for sustainable fuel and chemical production, *Cheminform* 46 (2015) 3259.
- [7] X. Chen, S. Shen, L. Guo, S.S. Mao, Semiconductor-based photocatalytic hydrogen generation, *Chem. Rev.* 110 (2010) 6503–6570.
- [8] T.P. Yoon, M.A. Ischay, J. Du, Visible light photocatalysis as a greener approach to photochemical synthesis, *Nat. Chem.* 2 (2010) 527.
- [9] K. Takanabe, Photocatalytic water splitting: quantitative approaches toward photocatalysis by design, *ACS Catal.* 7 (2017) 8006–8022.
- [10] X. Chen, L. Liu, P.Y. Yu, S.S. Mao, Increasing solar absorption for photocatalysis with black hydrogenated titanium dioxide nanocrystals, *Science* 331 (2011) 746–750.
- [11] Y. Shiraishi, H. Sakamoto, Y. Sugano, S. Ichikawa, T. Hirai, Pt-Cu bimetallic alloy nanoparticles supported on anatase TiO_2 : highly active catalysts for aerobic oxidation driven by visible light, *ACS Nano* 7 (2013) 9287–9297.

- [12] L. Mu, Y. Zhao, A. Li, S. Wang, Z. Wang, J. Yang, Y. Wang, T. Liu, R. Chen, J. Zhu, Enhancing charge separation on high symmetry SrTiO₃ exposed with anisotropic facets for photocatalytic water splitting, *Energy Environ. Sci.* 9 (2016) 2463–2469.
- [13] S. Chu, Y. Wang, Y. Guo, J. Feng, C. Wang, W. Luo, X. Fan, Z. Zou, Band structure engineering of carbon nitride: in search of a polymer photocatalyst with high photooxidation property, *ACS Catal.* 3 (2013) 912–919.
- [14] J. Zhang, M. Zhang, S. Lin, X. Fu, X. Wang, Molecular doping of carbon nitride photocatalysts with tunable bandgap and enhanced activity, *J. Catal.* 310 (2014) 24–30.
- [15] H. Wang, Y.J. Sun, G.M. Jiang, Y.X. Zhang, H.W. Huang, Z.B. Wu, S.C. Lee, F. Dong, Unraveling the mechanisms of visible light photocatalytic NO purification on earth-abundant insulator-based core-shell heterojunctions, *Environ. Sci. Technol.* 52 (2018) 1479–1487.
- [16] H. Wang, Y.J. Sun, W.J. He, Y. Zhou, S.C. Lee, Dong F, Visible light induced electron transfer from a semiconductor to an insulator enables efficient photocatalytic activity on insulator-based heterojunctions, *Nanoscale* 10 (2018) 15513–15520.
- [17] W.R. Leow, W.K.H. Ng, T. Peng, X.F. Liu, B. Li, W.X. Shi, Y.W. Lum, X.T. Wang, X.J. Lang, S.Z. Li, N. Mathews, J.W. Ager, T.C. Sum, H. Hirao, X.D. Chen, Al₂O₃ surface complexation for photocatalytic organic transformations, *J. Am. Chem. Soc.* 139 (2017) 269–276.
- [18] R.G. Li, X.L. Wang, S.Q. Jin, X. Zhou, Z.C. Feng, Z. Li, J.Y. Shi, Q. Zhang, C. Li, Photo-induced H₂ production from a CH₃OH-H₂O solution at insulator surface, *Sci. Rep.* 5 (2015) 13475.
- [19] F. Dong, T. Xiong, Y.J. Sun, L.J. Lu, Y.X. Zhang, H.J. Zhang, H.W. Huang, Y. Zhou, Z.B. Wu, Exploring the photocatalysis mechanism on insulators, *Appl. Catal. B: Environ.* 219 (2017) 450–458.
- [20] Z. Zhang, J.J. Yates, Band bending in semiconductors: chemical and physical consequences at surfaces and interfaces, *Chem. Rev.* 112 (2012) 5520.
- [21] A.L. Linsebigler, G.Q. Lu, J.Y. Yates, Photocatalysis on TiO₂ surfaces: principles, mechanisms, and selected results, *Chem. Rev.* 95 (1995) 735–758.
- [22] M. Heitbaum, F. Glorius, I. Escher, Asymmetric heterogeneous catalysis, *Angew. Chem. Int. Ed.* 45 (2010) 4732–4762.
- [23] R.I. Masel, Principles of adsorption and reaction on solid surfaces, *J. Catal.* 1 (1997) 214.
- [24] X.Q. Gong, A. Selloni, M. Batzill, U. Diebold, Steps on anatase TiO₂(101), *Nat. Mater.* 5 (2006) 665–670.
- [25] S. Wang, L. Pan, J.J. Song, W. Mi, J.J. Zou, L. Wang, X. Zhang, Titanium-defected undoped anatase TiO₂ with p-type conductivity, room-temperature ferromagnetism and remarkable photocatalytic performance, *J. Am. Chem. Soc.* 137 (2015) 2975–2983.
- [26] G. Li, G.R. Blake, T.T. Palstra, Vacancies in functional materials for clean energy storage and harvesting: the perfect imperfection, *Chem. Soc. Rev.* 46 (2017) 1693.
- [27] A.A. Finch, N. Allison, H. Steagles, C.V. Wood, J.F.W. Mosselmans, Ba XAFS in Ba-rich standard minerals and the potential for determining Ba structural state in calcium carbonate, *Chem. Geol.* 270 (2010) 179–185.
- [28] N. Zhang, X. Li, H. Ye, S. Chen, H. Ju, D. Liu, Y. Lin, W. Ye, C. Wang, Q. Xu, Oxide defect engineering enables to couple solar energy into oxygen activation, *J. Am. Chem. Soc.* 138 (2016) 8928–8935.
- [29] J. Xu, Y. Teng, F. Teng, Effect of surface defect states on valence band and charge separation and transfer efficiency, *Sci. Rep.* 6 (2016) 32457.
- [30] S. Yu, Y. Zhang, F. Dong, M. Li, T. Zhang, H. Huang, Readily achieving concentration-tunable oxygen vacancies in Bi₂O₂CO₃: triple-functional role for efficient visible-light photocatalytic redox performance, *Appl. Catal. B: Environ.* 226 (2018) 441–450.
- [31] S. Steinmann, S. Melissen, T.L. Bahers, P. Sautet, Challenges in calculating the bandgap of triazine-based carbon nitride structures, *J. Mater. Chem. A Mater. Energy Sustain.* 5 (2017) 5115–5122.
- [32] A. Yamamoto, Y. Mizuno, K. Teramura, S. Hosokawa, T. Tanaka, Noble-metal-free NO_x storage over Ba-modified TiO₂ photocatalysts under UV-light irradiation at low temperatures, *ACS Catal.* 5 (2015) 2939–2943.
- [33] A. Yamamoto, Y. Mizuno, K. Teramura, S. Hosokawa, T. Tanaka, Surface Ba species effective for photoassisted NO_x storage over Ba-modified TiO₂ photocatalysts, *Appl. Catal. B: Environ.* 180 (2016) 283–290.
- [34] R. Bader, *Atoms in Molecules: A Quantum Theory*, Oxford University Press, 1994.
- [35] T. Weingand, S. Kuba, K. Hadjivanov, H. Knözinger, Nature and reactivity of the surface species formed after NO adsorption and NO + O₂ coadsorption on a WO₃-ZrO₂ catalyst, *J. Catal.* 209 (2002) 539–546.
- [36] K. Hadjivanov, V. Avreyska, A. Dimitar Klissurski, T. Marinova, Surface species formed after NO adsorption and NO + O₂ coadsorption on ZrO₂ and sulfated ZrO₂: an FTIR spectroscopic study, *Langmuir* 18 (2002) 1619–1625.
- [37] Y. Zhou, Z. Zhao, F. Wang, K. Cao, D.E. Doronkin, F. Dong, Facile synthesis of surface N-doped Bi₂O₂CO₃: origin of visible light photocatalytic activity and *in situ* DRIFTS studies, *J. Hazard. Mater.* 307 (2016) 163–172.
- [38] M. Kantcheva, Identification, stability, and reactivity of NO_x species adsorbed on titania-supported manganese catalysts, *J. Catal.* 204 (2001) 479–494.
- [39] L. Zhong, Y. Yu, W. Cai, X. Geng, Q. Zhong, Structure-activity relationship of Cr/Ti-PILC catalysts using a pre-modification method for NO oxidation and their surface species study, *Phys. Chem. Chem. Phys.* 17 (2015) 15036.
- [40] S.J. Huang, A.B. Walters, M.A. Vannice, Adsorption and decomposition of NO on lanthanum oxide, *J. Catal.* 192 (2000) 29–47.
- [41] Y. Nosaka, A.Y. Nosaka, Generation and detection of reactive oxygen species in photocatalysis, *Chem. Rev.* 117 (2017) 11302–11336.